Surfaces and Interfaces 57 (2025) 105696

Contents lists available at ScienceDirect

Surfaces and Interfaces

journal homepage: www.sciencedirect.com/journal/surfaces-and-interfaces

Tuning the crystallization temperature of titanium dioxide thin films by incorporating silicon dioxide *via* supercycle atomic layer deposition

Carina Hedrich [a,*], Davy Deduytsche [b], Robin R. Petit [b], Tobias Krekeler [c], Jun Peng [a], Martin Ritter [c], Jolien Dendooven [b], Christophe Detavernier [b], Robert H. Blick [a], Robert Zierold [a]

[a] Center for Hybrid Nanostructures (CHyN), Universität Hamburg, Luruper Chaussee 149, 22761 Hamburg, Germany
[b] CoCooN Group, Department of Solid State Sciences, Ghent University, Krijgslaan 281/S1, 9000 Ghent, Belgium
[c] Electron Microscopy Unit (BeEM), Technische Universität Hamburg (TUHH), Eißendorfer Straße 42, 21073 Hamburg, Germany

ARTICLE INFO

Keywords:
Titanium dioxide
Crystallization
Phase transition
Atomic layer deposition

ABSTRACT

Titanium oxide-based nanomaterials are nowadays of great interest in various application fields such as optics, sensing, photocatalysis, and solar cells. Tuning their physical properties by tailoring the geometry or combining them with different materials further expands their applicability and even allows for the generation of new functionalities. The materials' crystalline phase also determines its properties and the crystallization behavior can be modified by doping or multilayering thin films with various materials. For instance, the combination of TiO_2 with silicon dioxide (SiO_2) renders these composites ideal candidates for coatings applied in harsh environments based on the high chemical and mechanical stability of both materials. Applying such coatings in optics, sensing, or photocatalysis require accurate prediction of the evolution of their properties and crystalline phase during heat treatments within the fabrication and application. Herein, we present the fabrication of SiO_2-incorporated TiO_2 thin films by supercycle atomic layer deposition (ALD). Specifically, TiO_2-SiO_2 multilayers with varying material ratios, TiO_2 thicknesses, and individual layer numbers as well as SiO_2-doped TiO_2 thin films are prepared. Their crystallization behavior is studied by *in situ* X-ray diffraction during thermal annealing. The structural properties of the composite materials are assessed by X-ray reflectivity, spectroscopic ellipsometry, and transmission electron microscopy before and after annealing. TiO_2-SiO_2 multilayers show increasing crystallization temperatures from amorphous TiO_2 to anatase with decreasing TiO_2 layer thickness from 50 nm to 4 nm and with increasing number of TiO_2 layers. Their layered structure is retained during annealing while the interfaces roughen slightly. SiO_2-doped TiO_2 thin films demonstrate increasing crystallization temperatures with increasing SiO_2 contents up to 10 %. The refractive index of these doped structures is tailored by the SiO_2 content. Detailed characterization of ALD deposited SiO_2-containing TiO_2 thin films could further expand their application in the future by precisely adjusting the fabrication process for the desired material properties and target application.

1. Introduction

Nanomaterials have gained significant attention over the past decades due to their unique and tunable properties, which find application in various technological fields [1,2]. Among these materials, titanium dioxide (titania, TiO_2) is a very versatile and promising semiconductor based on its optical, electronic, and photocatalytic properties [2–4]. TiO_2 thin films with layer thicknesses on the nanometer scale feature increased surface area-to-volume ratios whereby quantum effects occur and the film's electronic structure, band gap, and crystallographic phase transition behavior change depending on the thickness [2,4–7]. The crystallographic phase of TiO_2 – predominantly amorphous, anatase, rutile, or brookite – determines the materials' structural and functional properties, such as mechanical strength, optical properties, and thermal stability [8,9]. Hence, precise control over the crystallinity is crucial to tailor the properties of TiO_2 thin films for the desired application. Depending on the synthesis method, as-prepared TiO_2 thin films are crystalline or amorphous. The latter ones can be transformed into

* Corresponding author at: Center for Hybrid Nanostructures (CHyN), Universität Hamburg, Luruper Chaussee 149, 22761 Hamburg, Germany.
E-mail address: carina.hedrich@chyn.uni-hamburg.de (C. Hedrich).

https://doi.org/10.1016/j.surfin.2024.105696
Received 28 May 2024; Received in revised form 4 October 2024; Accepted 21 December 2024
Available online 22 December 2024

crystalline films by post-processing such as thermal annealing. Structural stabilization of TiO_2 thin films upon heat treatments and thus, modification of the crystallization behavior can be achieved by doping or multilayering the films with various materials. The incorporation of foreign atoms locally changes the structure of the TiO_2 thin films and therefore alters the crystallization process. For instance, doping of TiO_2 is reported to shift the crystallization temperature to higher temperatures [10–20]. Moreover, such approach influences the phase transition dynamics and can, *e.g.*, suppress the phase transition from anatase to rutile depending on the dopant material and concentration [15–17,20]. Furthermore, the deposition of multilayered structures, where TiO_2 is alternated with layers of other metal oxides creates interfaces influencing nucleation and growth dynamics [8,11,12,19,21–29]. These multilayers can control phase transformation processes, promote the formation of specific crystalline phases such as anatase or rutile, and tailor microstructural characteristics [8,11,19,22,24,27].

This combinatorial approach of doping and multilayering offers a versatile platform to further extend and customize the properties of TiO_2 thin films to suit the intended application [3]. For example, SiO_2 is an interesting material featuring a low refractive index at similar high chemical and mechanical stability as TiO_2 [14]. Thus, multilayers of TiO_2 and SiO_2 can be utilized in different fields such as optics, sensing, thermal barrier coatings, or photocatalysis, to name a few [8,19,21,22,24,25,30–32]. Previous reports about TiO_2-SiO_2 multilayers observed a thickness dependence of the crystallization temperature on the TiO_2 film thickness ranging from 4 nm to several hundred nanometers [19,21–26]. This correlation arises from the increasing influence of the surface and interface energies onto the crystallographic phase transition with increasing surface area-to-volume ratio of the TiO_2 films, *i.e.*, with decreasing film thickness [19,22]. These studies utilized *ex situ* characterization techniques after annealing the structures at varying temperatures to investigate the crystallization behavior. To precisely determine the crystallization onset, *in situ* characterization during the thermal annealing would be required but was not reported so far for TiO_2-SiO_2 multilayer thin films. Apart from TiO_2-SiO_2 multilayers, doping of TiO_2 with SiO_2 presents another possibility to tune the temperature-dependent structural properties. Homogeneously doped films containing TiO_2 and SiO_2 showed composition-dependent crystallization behavior [13–18]. The increase of the TiO_2 crystallization temperature with increasing SiO_2 content can be explained by raised activation energies for the crystallization because additional Si atoms interact strongly with the TiO_2 lattice [14,16,18]. However, both types of SiO_2-incorporated TiO_2 films, *i.e.*, TiO_2-SiO_2 multilayers and SiO_2-doped TiO_2, were prepared by sputtering, sol-gel chemistry, chemical vapor deposition, physical vapor deposition, or wet-chemical synthesis. These deposition techniques face limitations regarding coating conformality on complex-shaped substrates and/or precision of the film thickness control.

To overcome these limitations, atomic layer deposition (ALD) is utilized in this work to produce TiO_2-SiO_2 multilayers and SiO_2-doped TiO_2 thin films. ALD is a gas phase deposition technique that allows for precise thickness control of deposited films on the Ångström scale through sequential self-limiting reactions between gaseous precursors and solid surfaces [33,34]. Thus, three-dimensional or complex-shaped substrates can also be conformally coated by ALD. Furthermore, the combination of different materials in one ALD deposition process can be easily realized by supercycles [34,35]. These supercycles consist of pre-defined numbers of ALD cycles for the different materials carried out consecutively as schematically shown in Fig. 1(a). The desired film thickness per material is obtained by tuning the ALD cycle numbers within the supercycle. In this way, tailored multilayers can be produced by alternating the deposition processes for the different materials. On the other hand, doping of materials is possible by periodically introducing single ALD cycles of the dopant material into the ALD process of the host material [36]. Hence, the properties of the deposited material can be precisely tailored by applying supercycle ALD processes.

Herein, we report on the fabrication of TiO_2-SiO_2 multilayers and SiO_2-doped TiO_2 thin films *via* supercycle ALD. The crystallization behavior of the nanometer thin TiO_2 films is investigated by *in situ* and *ex situ* X-ray diffraction (XRD) during thermal annealing of the structures. Specifically, shifting of the TiO_2 crystallization to higher temperatures with decreasing layer thickness and increasing number of material interfaces is studied in TiO_2-SiO_2 multilayers. Composition-dependent crystallization properties are also observed in SiO_2-doped TiO_2 thin films. In addition, the structural appearance of the composite materials is characterized by X-ray reflectivity (XRR) measurements before and after the annealing. Furthermore, cross-section transmission electron microscopy (TEM) images of TiO_2-SiO_2 multilayers reveal that the layered structure is retained but roughened after thermal annealing. Spectroscopic ellipsometry of SiO_2-doped TiO_2 thin films was used to investigate the change of the refractive index upon annealing.

2. Experimental section

2.1. Materials

P-doped silicon wafers with native SiO_2 layers (thickness 1.4–1.7 nm) were supplied by Siegert Wafer (Germany). Titanium tetraisopropoxide (TTIP, CAS 546–68–9), tris(dimethlamino)silane (TDMAS, CAS 15,112–89–7), acetone (CAS 67–4–1), and isopropyl alcohol (IPA,

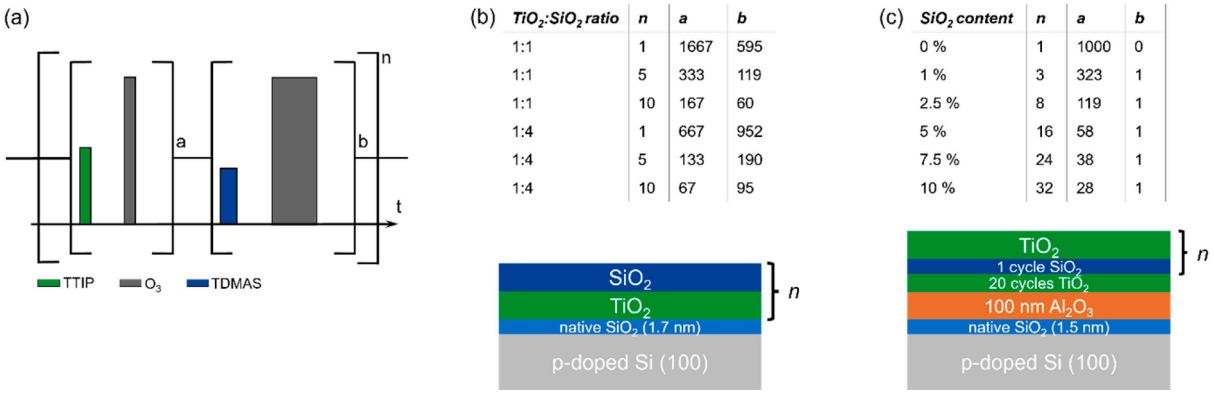

Fig. 1. (a) Schematic structure of a supercycle ALD process. The first material (TiO_2) forms by reactions of TTIP and O_3. The cycles are repeated *a* times until the desired thickness is reached. The second material (SiO_2) is deposited in *b* cycles of TDMAS and O_3. Both cycles are repeated *n* times as a supercycle. (b) Composition of alternating TiO_2-SiO_2 multilayers and the respective cycle numbers *a, b*, and the supercycle numbers *n* applied for the samples presented in this publication. (c) SiO_2-doped TiO_2 thin films are prepared by introducing single SiO_2 deposition cycles between varying amounts of TiO_2 cycles to achieve different doping ratios. The process parameters are presented, and the structure of the films on top of a Al_2O_3-coated substrate is depicted.

CAS 67–63–0) were purchased from Sigma Aldrich (Germany). Trimethylaluminum (TMA, CAS 75–24–1) was supplied by Strem Chemicals (France). Milli-Q water (> 16 MΩ cm, H_2O) was used as deionized water (DI-H_2O). Oxygen (5.0) and nitrogen (6.0) were received from Westfalen Gas and SOL, respectively.

2.2. Fabrication

TiO_2-SiO_2 multilayers and SiO_2-doped TiO_2 films were prepared by supercycle ALD processes (Fig. 1a). Silicon wafer pieces were cleaned in acetone and IPA followed by drying under N_2 steam for both sample sets. TiO_2 and SiO_2 ALD processes were conducted in a GEMStar XT™ system (Arradiance, USA) under stop-flow conditions. Both materials were deposited at 150 °C in a constant N_2 flow of 30 sccm. Ozone (O_3) generated by an R-Lab 112 ozone generator (Pacific Ozone, USA) was utilized as oxygen precursor for both processes. TTIP heated to 80 °C and TDMAS at 40 °C were used as titanium and silicon precursor, respectively. The pulse, exposure, and purge times of the individual ALD half-cycle during the TiO_2 process were as following: 0.1 s, 10 s, and 30 s for TTIP and 2 s, 10 s, and 30 s for O_3. SiO_2 deposition was conducted with pulse, exposure, and purge times of 0.05 s, 15 s, and 30 s for TDMAS and 2 s, 40 s, and 30 s for O_3. The growth per cycle (GPC) was 0.3 Å for TiO_2 and 0.84 Å for SiO_2 deposition in agreement with existing literature [37–40]. TiO_2-SiO_2 multilayers were deposited on cleaned Si wafers. The TiO_2:SiO_2 ratio and individual layer thicknesses were tuned by varying the TiO_2 and SiO_2 deposition cycles (*a* and *b*) as well as the supercycle number (*n*). All supercycle processes were designed to receive a total coating thickness of 100 nm. Note, the individual cycle and supercycle numbers of the samples investigated are summarized in Fig. 1b. Two different TiO_2:SiO_2 ratios are deposited to test their effect on the crystallization behavior based on the different surface area-to-volume ratio in the layers. A 45 nm pure TiO_2 thin film was prepared on a clean Si wafer by applying 1500 TiO_2 ALD cycles.

SiO_2-doped TiO_2 thin films are fabricated on Si wafer pieces which were previously coated with 100 nm Al_2O_3 by ALD as diffusion barrier to prevent unintended Si-doping of the TiO_2 film by the substrate [41,42]. The alumina ALD process was performed in a home-built ALD system under stop-flow conditions at 150 °C. TMA and DI-H_2O were used as precursors with pulse, exposure, and purge times for both of 0.05 s, 5 s, and 45, respectively. 625 cycles were applied to obtain a film thickness of 100 nm. Deposition of SiO_2-doped TiO_2 was conducted in the Arradiance GEMStar system under the same process conditions as described above for the multilayer structures. One SiO_2 cycle was applied within one supercycle to fabricate SiO_2-doped TiO_2. To ensure a constant base layer, 20 cycles of TiO_2 were applied before starting the supercycle process. The TiO_2:SiO_2 ratio and number of supercycles were varied to tailor the SiO_2 percentage while keeping the total film thickness constant at 30 nm. The process parameters are shown in Fig. 1c.

2.3. Characterization

TiO_2-SiO_2 multilayers and SiO_2-doped TiO_2 films were structurally characterized by *in situ* X-ray diffraction (XRD) during thermal annealing. A Bruker (USA) D8 discover X-ray diffractometer equipped with a home-built annealing chamber (Ghent University) was utilized. Copper Kα radiation was applied, and the samples were annealed in ambient air at a heating rate of 10 °C/min up to 900 °C. *In situ* XRD scans in the range of 20° to 40° were taken with an integration time of 15 s. Data processing of the *in situ* data emphasizes signals with low intensities in order to be able to distinguish them from the background in the color maps. Occasionally, this processing causes signals at the measuring range's edge to be overly amplified. Note, artefacts do not appear in the *ex situ* measurements, which serve as control. Before and after the annealing, a full angle *ex situ* scan from 15° to 65° with a resolution of 0.05°, an offset of 5°, and 4 s integration time was taken for each sample. X-ray reflectivity (XRR) patterns of TiO_2-SiO_2 multilayers and SiO_2-doped TiO_2 films were measured before and after annealing in a Bruker D8 discover system employing Cu Kα radiation. XRR measurements were recorded from 0.2° to 4.0° with a step size of 0.01° and an integration time of 1 s per step. Transmission electron microscopy (TEM) images of TiO_2-SiO_2 multilayer cross-sections were acquired with a Thermo Fisher (Germany) Talos F200X in BF and HAADF-Mode. Sample preparation was done with a Thermo Fisher Helios G3UC Focused Ion Beam (FIB) using a standard *in situ* lift-out technique of the FIB lamellae. Spectroscopic ellipsometry characterization for the SiO_2-doped TiO_2 thin films are carried out with a SENpro ellipsometer by SENTECH (Germany). Specifically, Cauchy models have been used to analyze Al_2O_3 as substrate coating material and SiO_2-doped TiO_2 films. Atomic force microscopy (AFM) measurements of SiO_2-doped TiO_2 films were conducted with a Dimension 3100 Atomic Force Microscope (Bruker, USA).

3. Results and discussion

3.1. TiO_2-SiO_2 multilayers

The crystallization temperature of ALD-deposited TiO_2 thin films can be tailored by incorporating SiO_2 either as TiO_2-SiO_2 multilayer structures or by SiO_2-doping. All films are amorphous after deposition and annealing is necessary to induce crystallization. Crystallization from the amorphous TiO_2 phase into polycrystalline anatase films is observed by *in situ* XRD measurements for layer thicknesses between 4 nm and 50 nm (Fig. 2, **left column**). Note, silica remains amorphous for all heat treatments performed in this study in agreement with the literature [21, 43]. For the multilayers, the crystallization temperature T_{cr} of TiO_2 increases with decreasing thickness of the individual TiO_2 layers within the stack. Note, TiO_2 layers in both investigated TiO_2:SiO_2 thickness ratios of 1:1 and 1:4 with varying individual layer thicknesses transform into anatase. While a crystallization temperature of 405 °C is observed for the 50 nm TiO_2 film, it increases up to 475 °C for a TiO_2-SiO_2 multilayer with 4 nm individual TiO_2 layer thickness as summarized in Fig. 3. The anatase (101) peak at 25.7° is visible in the *in situ* XRD plots at temperatures above the crystallization temperature. The T_{cr} is denoted above each plot and marked by a grey line for each sample's plot. Increasing the supercycle number *n* with a fixed total film thicknesses result in two aspects that affect the crystallization temperature:

First, the individual TiO_2 thickness per layer is decreasing. Consequently, the interface area-to-volume ratio in these thin films is increasing whereby the influence of the interfaces becomes more prominent for the layer's properties [19,22]. Such a reduction in film thickness also restricts the crystallite sizes. Hence, it leads to a broadening of the peaks which is particularly visible in the *ex situ* XRD measurements [7]. By utilizing the peaks' full width at half maximum (FWHM), crystallite sizes were estimated from the anatase (101) peak by the Scherrer equation using a shape factor of 0.9 [44]. The results are summarized in Table 1 and reveal that crystallite sizes are in the range of the film thicknesses for layers thinner than 20 nm. The 50 nm thick TiO_2 film consists of crystallites with an average size of 25.2 nm. This observation indicates that for thicker layers (> 25 nm) the crystallite size upon annealing in our experimental setup is not influenced anymore by the confinement.

Second, the number of TiO_2-SiO_2 interfaces raises which further enhances the influence of the interfaces onto the properties of the overall structure [22]. Based on the different interface energies of amorphous TiO_2 and crystalline TiO_2 with amorphous SiO_2, Durante *et al.* calculated that the crystalline TiO_2 interface is energetically less favorable [22]. Note, T_{cr} for the 2 nm thick TiO_2 layers could not be clearly determined from the *in situ* data and is thus not included in Fig. 3. However, the *ex situ* data after the thermal annealing (Fig. 2g) shows a broad peak with low intensity at 25.8° indicating the anatase (101) peak. Note that the *in situ* measured intensity for this peak is below the detection limit of the XRD setup for such, only a few nanometers thin, film. Follow-up experiments can utilize synchrotron radiation to further quantify the

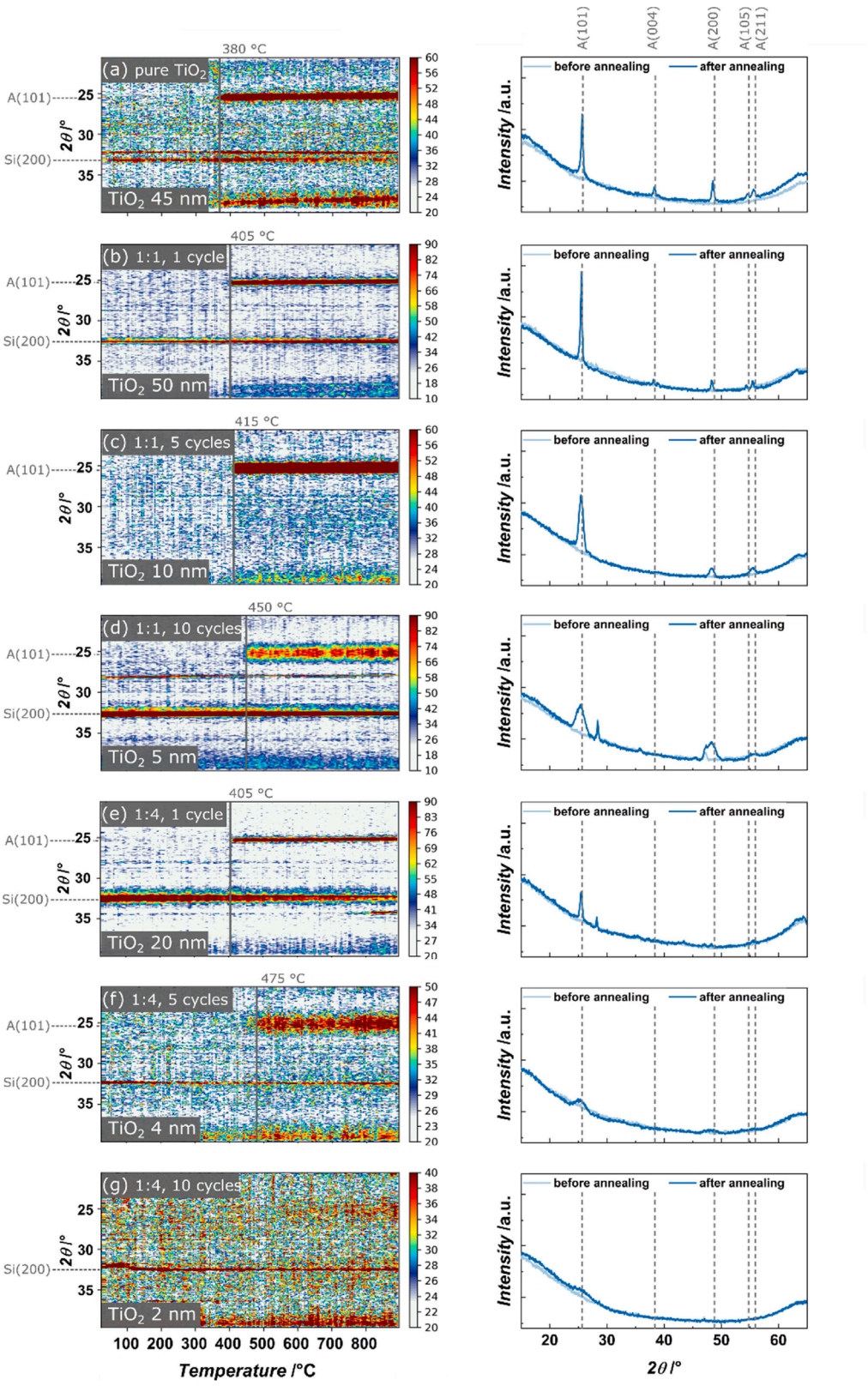

Fig. 2. *In situ* (left) and *ex situ* (right) XRD patterns of TiO_2-SiO_2 multilayers. In (a) the XRD patterns of a pure 45 nm TiO_2 film as reference are shown. The TiO_2:SiO_2 ratio is varied between 1:1 (b-d) and 1:4 (e-g) while the total film thickness is kept constant. The TiO_2 layers crystallize in anatase phase and the crystallization temperature (marked by the grey line in the *in situ* patterns) increases with decreasing TiO_2 film thickness. Peak positions for anatase 'A' (COD 1,010,942) are shown in the ex situ patterns in the right column. TiO_2 layer thicknesses of (b) 50 nm, (c) 10 nm, (d) 5 nm, (e) 20 nm, (f) 4 nm, and (g) 2 nm are investigated.

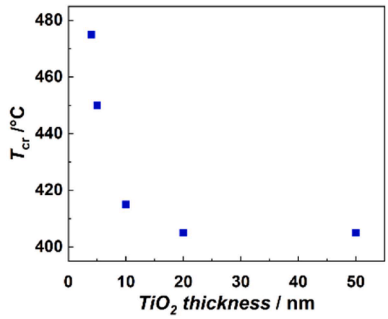

Fig. 3. The crystallization temperature T_{cr} of TiO_2 layers in TiO_2-SiO_2 multilayers increases with decreasing TiO_2 layer thickness.

Table 1
Crystallite sizes in the TiO_2 layers are calculated from the anatase (101) peak utilizing the Scherrer equation.

TiO_2 layer thickness /nm	FWHM /°	2θ /°	Crystallite size /nm
4	1.90	25.39	4.7
5	1.52	25.39	5.9
10	0.84	25.50	10.6
20	0.46	25.50	19.3
50	0.35	25.54	25.2

presence of anatase phase in TiO_2 layers below 4 nm.

As a control, the pure TiO_2 layer (Fig. 2a) shows a crystallization onset at 380 °C. This temperature is even below the measured value for a 50 nm TiO_2 thin film in a bilayer structure (405 °C). We conclude that any overcoating of TiO_2 by SiO_2 affects the crystallization behavior of TiO_2. As explained above, the additional interface energy effectively hinders the crystallization of the TiO_2 layer. Hence, the phase transition in such TiO_2-SiO_2 bilayers needs more energy than in an uncovered TiO_2 resulting in a higher T_{cr}.

In general, the TiO_2-SiO_2 multilayers are structurally stable upon thermal annealing. The film thicknesses, surface roughnesses, and interface roughnesses change only slightly after annealing the TiO_2-SiO_2 stack structures as revealed by the XRR patterns (Fig. 4). The observed minor modifications are caused by the TiO_2 phase transition and the corresponding rearrangement of atoms [17]. For better comparison, XRR patterns before and after annealing for each sample are shown in Fig. S1. The individual XRR plots were not fitted quantitatively due to the large number of individual layers, which led to a huge dimensionality of fit parameters, but the data is compared qualitatively. Oscillation periodicities increase slightly corresponding to decreasing film thicknesses caused by the densification and crystallization of the TiO_2 layers into the anatase phase [17]. Minor reductions of the oscillation amplitude after annealing suggest that the interfaces roughen slightly [45]. These results are corroborated by TEM analyses before and after thermal annealing (Fig. 5) revealing also the thickness decrease and indicating an increase in the surface roughness.

Specifically, the cross-section TEM images (Fig. 5) demonstrate that the TiO_2-SiO_2 multilayers retain their layered structure upon annealing. Analysis of the individual layer thicknesses was performed by using the software Fiji[46] and the results are summarized in Table 2. Individual layer thicknesses decrease by below 1 nm after the annealing up to 900 °C and the total film thicknesses reduce between 1.5 nm and 9.7 nm depending on the TiO_2:SiO_2 thickness ratio and the supercycle numbers. Furthermore, the TEM analysis supports the *ex situ* XRD measurements showing that TiO_2 and SiO_2 layers are amorphous before annealing. In contrast, after the thermal annealing, TiO_2 layers consist of crystalline grains with different orientation of the crystal lattices (Fig. 5b). This again is in good agreement with the multiple anatase peaks observed by *ex situ* XRD measurements (Fig. 2).

3.2. SiO_2-doped TiO_2 thin films

It was previously reported that utilization of aluminum-doped TiO_2 layers stabilizes the 1D and 3D photonic structures while simultaneously maintaining the high refractive index of the TiO_2 layers [10,11]. This prework motivated us to study the crystallization properties of supercyclic deposited SiO_2-doped TiO_2 thin films. Silica doping of TiO_2 films is obtained by applying single SiO_2 ALD cycles after a certain number of TiO_2 cycles in supercycle processes. Based on the cyclic nature of the ALD process, the dopant material SiO_2 is introduced as sub-monolayers in between TiO_2 layers. Hence, the structure resembles a delta-doped material characterized by the layered arrangment of host and dopant material with multiple regions of high dopant concentration within narrow profiles along the cross-section [47]. When the total film thickness is kept constant for the ALD process, the SiO_2 content raises with the total number of SiO_2 cycles within the ALD process. Each SiO_2

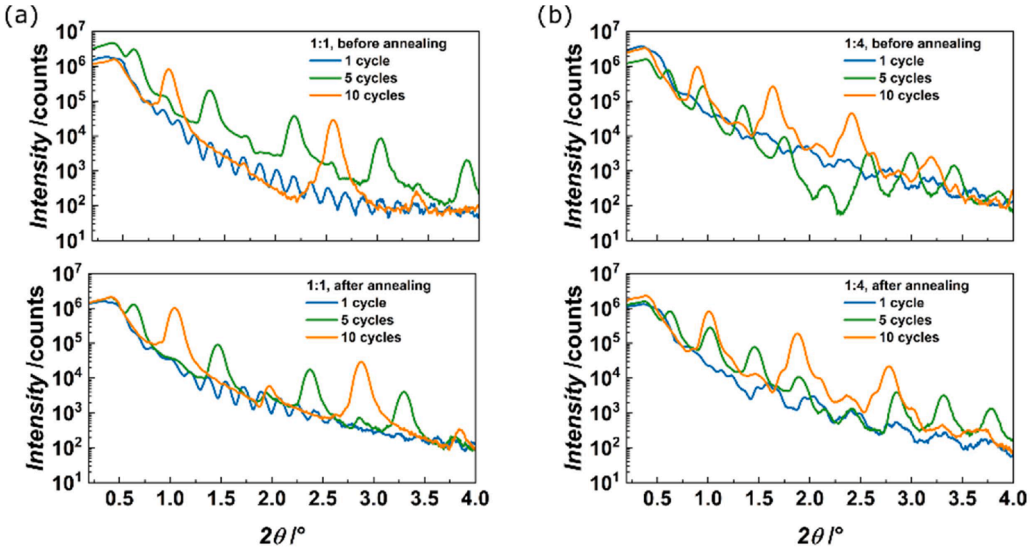

Fig. 4. XRR patterns of TiO_2-SiO_2 multilayers before and after annealing demonstrate that the film thicknesses, surface roughnesses, and interface roughnesses change only slightly. Multilayers fabricated with different ALD supercycle numbers are depicted for TiO_2:SiO_2 ratios of 1:1 (a) and 1:4 (b). Direct qualitative comparison of the same multilayer before and after annealing is presented in Fig. S1.

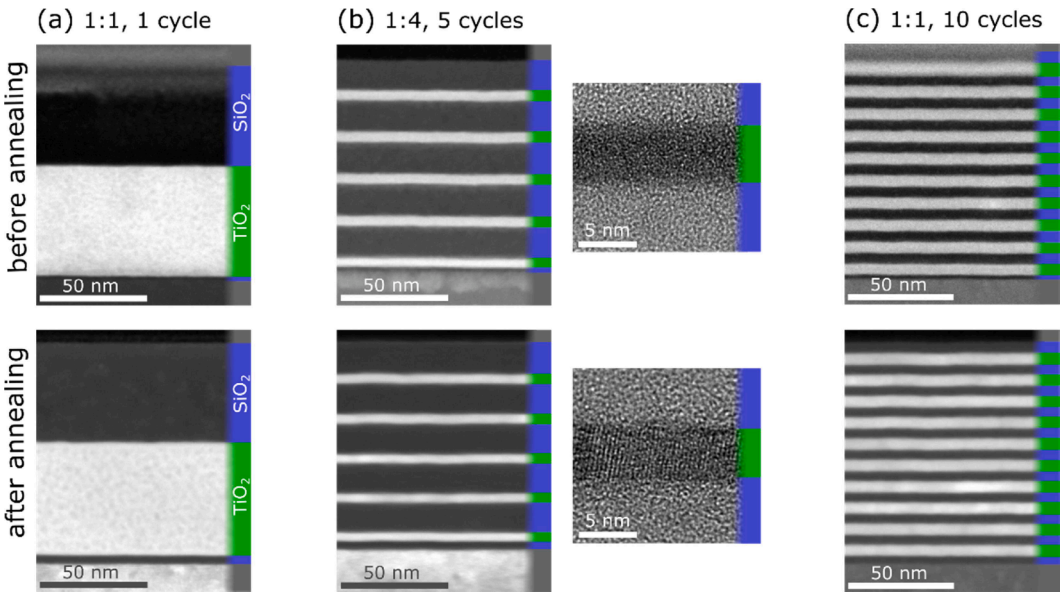

Fig. 5. Cross-sectional TEM images of different TiO_2-SiO_2 multilayers before and after thermal annealing. TEM micrographs before and after annealing (large images of a,b and c) were taken with an HAADF detector in STEM-mode. Here, TiO_2 is displayed in light grey while the SiO_2 layers are dark grey. The TEM images in higher magnification in (b) are HRTEM-images revealing an amorphous TiO_2 layer before annealing and showing lattice planes in the TiO_2 layer after annealing. The TiO_2 and SiO_2 layers are marked in green and blue on the right side of each image, respectively. Note, the thin bottom SiO_2 layers are native silicon dioxide layers of the substrate.

Table 2
Film thicknesses of the individual layers in TiO_2-SiO_2 multilayers analyzed by cross-section TEM images.

Sample	TiO_2 layer thickness /nm		SiO_2 layer thickness /nm		Total film thickness /nm	
	before annealing	after annealing	before annealing	after annealing	before annealing	after annealing
TiO_2:SiO_2 1:1, 1 supercycle	51.4 ± 0.5	50.5 ± 0.5	43.8 ± 0.5	43.2 ± 0.5	95.2 ± 0.5	93.7 ± 0.5
TiO_2:SiO_2 1:4, 5 supercycles	4.9 ± 0.5	4.3 ± 0.4	14.6 ± 0.3	14.5 ± 0.4	96.0 ± 0.5	94.1 ± 0.5
TiO_2:SiO_2 1:1, 10 supercycles	5.5 ± 0.2	5.3 ± 0.42	4.8 ± 0.2	4.0 ± 0.4	102.6 ± 0.5	92.9 ± 0.5

cycle alters the local bonding environment of titanium and oxygen in the TiO_2 film by creating material defects. As discussed above, the introduction of such additional material defects hinders the crystallization of the TiO_2 film during the thermal annealing. Note, an ALD-grown Al_2O_3 layer was deposited as diffusion barrier between the Si substrate and the SiO_2-doped TiO_2 thin film to prevent unintended Si-doping from the substrate [41,42]. Increasing the SiO_2 content in SiO_2-doped TiO_2 thin films leads to a rise of the crystallization temperature as shown in Fig. 6. T_{cr} to the anatase phase increases with the SiO_2 content from 420 °C for 0 % doping until 485 °C for a SiO_2 content of 10 %. *Ex situ* XRD analysis, exemplarily displayed for 7.5 % SiO_2 (Fig. 6g) proves that only the anatase phase is detected and no traces for rutile or brookite can be identified. The *ex situ* XRD data of the other samples are depicted in Fig. S2. The observed linear trend between 1 % and 10 % SiO_2 content (Fig. 6h) is in good agreement with a previous study by Waleczek *et al.* on the influence of Al_2O_3 doping by supercycle ALD on T_{cr} of TiO_2 films [10].

The high refractive index of TiO_2 is a key feature, which is mitigated by excessive doping with a lower refractive index material. We used spectroscopic ellipsometry data (Fig. 7**a**) to determine the refractive index as a function of SiO_2 content as-prepared and upon annealing. Note, by employing the supercycle approach, the refractive index can be precisely tailored because the amount of SiO_2 can be finely adjusted. Refractive indices presented in Fig. 7a are measured at SiO_2-doped TiO_2 samples featuring the same SiO_2 contents but prepared directly on silicon wafers without the Al_2O_3 diffusion barrier to reduce the number of fitting parameters for the analysis. Upon annealing at temperatures above the crystallization, an increase of the refractive index of the SiO_2-doped TiO_2 films is observed. Such an increase in refractive index is expected due to the TiO_2 film crystallization into the anatase phase [8,9]. Spectroscopic ellipsometry results of the samples with Al_2O_3 barrier layer are depicted in Fig. S3 and reveal a similar behavior. The XRR measurements of the samples are very similar before and after thermal annealing (Fig. 7b-d and Fig. S4). We therefore conclude, that the film thicknesses of SiO_2-doped TiO_2 films remain almost constant after annealing. However, the reflected intensity decays faster after the annealing. Such behavior could be related to an increase of the surface roughness of the SiO_2-doped TiO_2 films as confirmed by atomic force microscopy measurements (Table 3 and Fig. S5) [8,45]. Note, a significant difference in crystallization temperature is identified when comparing the reference sample containing 0 % doping with the results of the pure TiO_2 sample (shown in Fig. 2a). We attribute this mismatch to the different substrates.

3.3. *Influence of the substrate surface*

The annealing results of the reference substrates for both types of samples, *i.e.*, multilayers and doped TiO_2 thin films differ. This observation obviously demonstrates that also the utilized substrate affects the crystallization behavior besides multilayering or doping of TiO_2. For the mutlilayer samples, cleaned silicon wafer pieces with 1.7 nm native SiO_2 were directly used as substrates; whereas the SiO_2-doped TiO_2 structures were fabricated on silicon wafer pieces previously coated with 100 nm aluminum oxide (Al_2O_3) by ALD. Although the pure TiO_2 film prepared on the Al_2O_3-coated substrates, *i.e.*, 0 % SiO_2 content in TiO_2, has a thickness of 30 nm, its crystallization temperature of 420 °C (Fig. 6a)

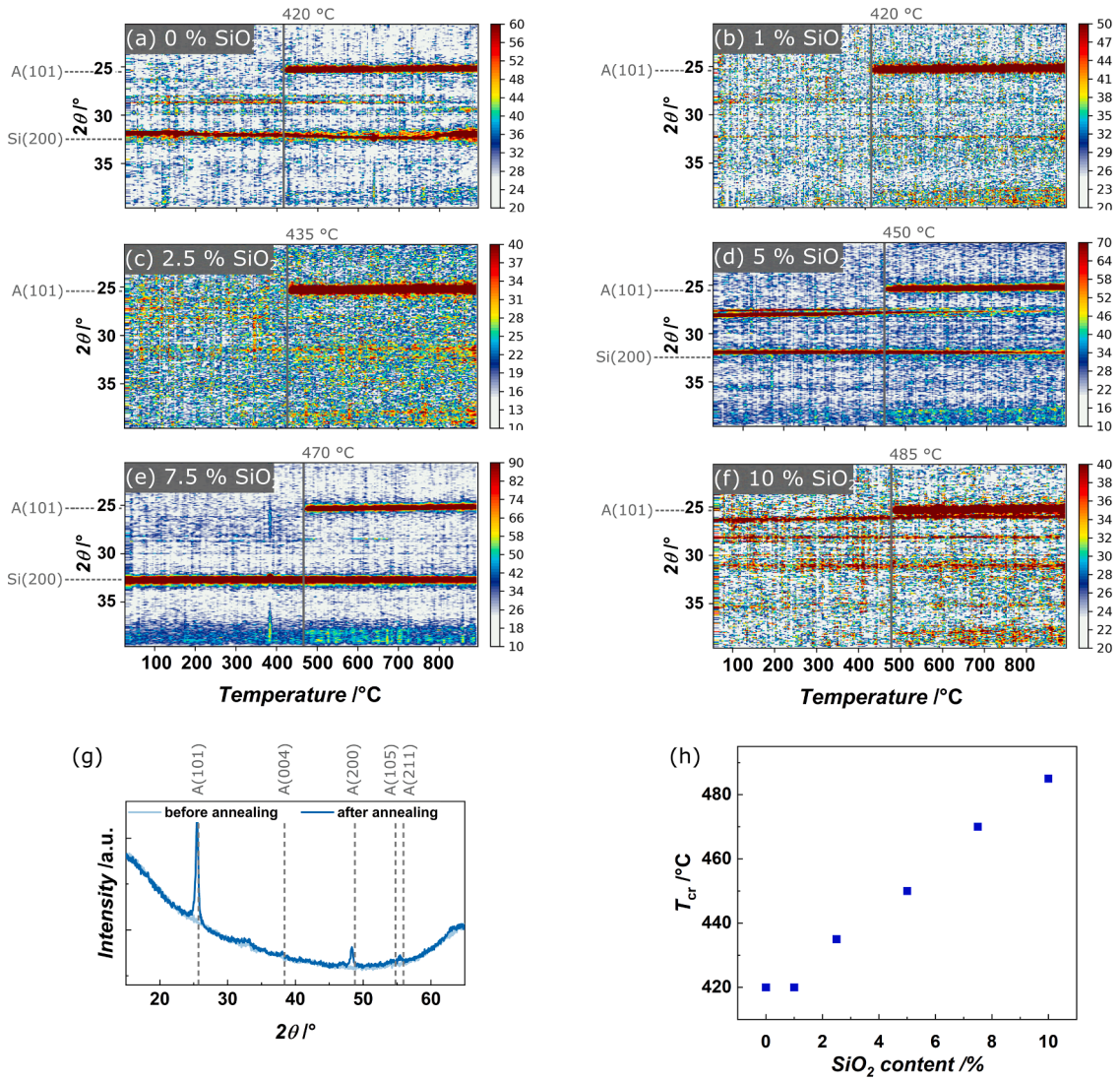

Fig. 6. XRD studies of SiO_2-doped TiO_2 thin films with varied SiO_2 content. (a-f) *In situ* XRD patterns of SiO_2 contents 0 %, 1 %, 2.5 %, 5 %, 7.5 %, and 10 %. The crystallization temperature of anatase formation is inidcated by the grey line. (g) *Ex situ* XRD measurement of the TiO_2 film containing 7.5 % SiO_2 before and after annealing showing the crystallization into anatase phase ('A', COD 1,010,942). (h) The crystallization temperature increases with increasing SiO_2 content.

exceeding the values from the thickness dependence observed for the TiO_2-SiO_2 multilayers (405 °C, Fig. 3) and for 45 nm pure TiO_2 (380 °C, Fig. 2a). Since different materials are utilized as substrate layers in direct contact with the TiO_2 thin film, the interface energies differ. Durante *et al.* reported on a higher interface energy for TiO_2 in contact with Al_2O_3 than with SiO_2 [22]. As a consequence, more energy is required for the phase transition from amorphous TiO_2 to anatase when an Al_2O_3--functionalized substrate is used resulting in a higher T_{cr} as observed in our experiments.

4. Conclusion

The crystallization temperature of ALD-deposited TiO_2 from the amorphous to the anatase phase depends on the incorporation of SiO_2 in the form of a multilayer structure or as delta-doping. Specifically, T_{cr} increases with decreasing thickness of individual TiO_2 layers embedded in SiO_2 layers. In both cases, the influence of material interfaces between TiO_2 and SiO_2 layers becomes more dominant for the phase transition. In accordance with this, T_{cr} increases when the SiO_2 content is raised in SiO_2-doped TiO_2 films. Both, TiO_2-SiO_2 multilayers and SiO_2-doped TiO_2 films retain their structural properties after thermal annealing. Minor changes of thicknesses, surface roughnesses, and interface roughnesses can be attributed to the rearrangement of atoms caused by the TiO_2 phase transition.

The systematic study of the crystallization temperature in SiO_2 containing TiO_2 films allows for precise adjustment of annealing temperatures to obtain or to prevent the crystallization of nanometer thin TiO_2 films. By controlling the delta-doping of SiO_2, the refractive index in SiO_2-doped TiO_2 thin films can be tailored. Speaking in terms of generality, fabricating such multilayered or doped structures by ALD enables their application to a wide range of templates not accessible with other deposition techniques such as highly porous structures or three-dimensional complex-shaped templates. On the one hand, the very precise thickness control of ALD processes might pave the way for further reduction of the individual layer thicknesses and hence, for a further increase of the TiO_2 crystallization temperature. On the other hand, such doped materials can, for example, be utilized in photocatalysis because they decrease the optical bandgap of TiO_2 and ease the charge carrier generation [15,16]. In this context, precise knowledge of the increased crystallization temperature is essential as the crystalline anatase phase has a higher photocatalytic activity than amorphous TiO_2 and hence, anatase is desired to be obtained by thermal annealing [48–50].

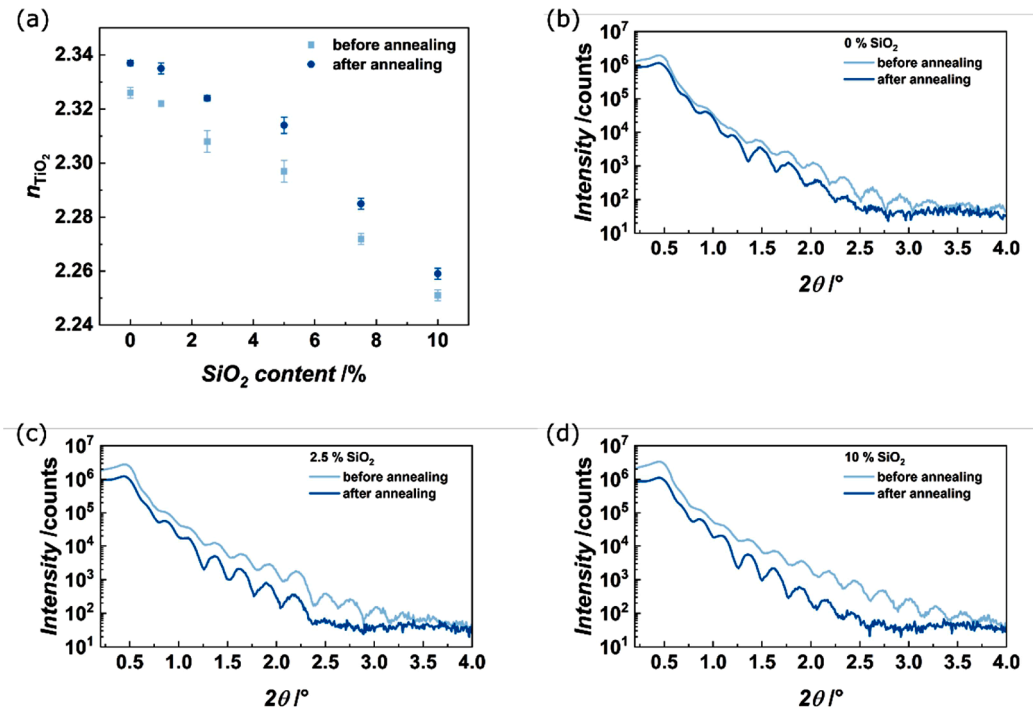

Fig. 7. (a) TiO_2 refractive index n of the SiO_2-doped TiO_2 films determined by spectroscopic ellipsometry at 632.8 nm wavelength. The SiO_2 content tailors the refractive index of the TiO_2 films. The refractive indices increase for all samples after annealing. (b-d) XRR patterns of SiO_2-doped TiO_2 thin films before and after annealing. The patterns are exemplary shown for SiO_2 contents of (b) 0 %, (c) 2.5 %, and (d) 10 %. The XRR data of 1 %, 5 %, and 7.5 % SiO_2 content are displayed in Fig. S4.

Table 3
Surface roughness of SiO_2-doped TiO_2 thin films measured by atomic force microscopy.

SiO_2 content	Surface roughness /nm	
	Before anneling	After annealing
0	0.41	0.91
1	0.19	1.15
2.5	0.36	2.43
5	0.42	2.18
7.5	0.44	2.35
10	0.26	3.27

CRediT authorship contribution statement

Carina Hedrich: Writing – original draft, Visualization, Methodology, Investigation, Formal analysis, Data curation, Conceptualization. **Davy Deduytsche:** Writing – review & editing, Visualization, Methodology, Investigation, Formal analysis, Data curation. **Robin R. Petit:** Writing – review & editing, Methodology, Investigation, Formal analysis, Data curation. **Tobias Krekeler:** Writing – review & editing, Methodology, Investigation, Data curation. **Jun Peng:** Writing – review & editing, Methodology, Investigation, Formal analysis, Data curation. **Martin Ritter:** Writing – review & editing, Supervision, Funding acquisition. **Jolien Dendooven:** Writing – review & editing, Supervision, Resources, Project administration, Funding acquisition. **Christophe Detavernier:** Writing – review & editing, Supervision, Resources, Project administration, Funding acquisition. **Robert H. Blick:** Writing – review & editing, Supervision, Resources, Project administration, Funding acquisition. **Robert Zierold:** Writing – review & editing, Writing – original draft, Validation, Supervision, Resources, Project administration, Funding acquisition, Conceptualization.

Declaration of competing interest

The authors declare the following financial interests/personal relationships which may be considered as potential competing interests: Carina Hedrich, Tobias Krekeler, Jun Peng, Martin Ritter, Robert H. Blick, and Robert Zierold report financial support was provided by German Reserach Foundation. Davy Deduytsche, Robin R. Petit, Jolien Dendooven, and Christophe Detavernier report financial support was provided by Ghent University. If there are other authors, they declare that they have no known competing financial interests or personal relationships that could have appeared to influence the work reported in this paper.

Acknowledgements

Authors would like to acknowledge funding by the Deutsche Forschungsgemeinschaft (DFG) within the Collaborative Research Initiative SFB 986 “Tailor-Made Multi-Scale Materials Systems” (project number 192346071) and by the special research fund BOF of Ghent University (BOF-GOA, 01G01019). We acknowledge financial support from the Open Access Publication Fund of Universität Hamburg.

Supplementary materials

Supplementary material associated with this article can be found, in the online version, at doi:10.1016/j.surfin.2024.105696.

Data availability

Data will be made available on request.

References

[1] M. Benelmekki, Nanomaterials The Original Product of Nanotechnology, Morgan & Claypool Publishers, San Rafael, California, 2019.

[2] N. Kumar, S. Kumbhat, Essentials in Nanoscience and Nanotechnology, John Wiley & Sons Inc., Hoboke, New Jersey, 2016.

[3] M. Dahl, Y. Liu, Y. Yin, Composite titanium dioxide nanomaterials, Chem. Rev. 114 (19) (2014) 9853–9889, https://doi.org/10.1021/cr400634p.

[4] X. Chen, S.S. Mao, Titanium dioxide nanomaterials: synthesis, properties, modifications, and applications, Chem. Rev. 107 (7) (2007) 2891–2959, https://doi.org/10.1021/cr0500535.

[5] T. Guang-Lei, H. Hong-Bo, S. Jian-Da, Effect of microstructure of TiO $_2$ thin films on optical band gap energy, Chin. Phys. Lett. 22 (7) (2005) 1787–1789, https://doi.org/10.1088/0256-307X/22/7/062.

[6] M. Tallarida, C. Das, D. Schmeisser, Quantum size effects in TiO $_2$ thin films grown by atomic layer deposition, Beilstein J. Nanotechnol. 5 (2014) 77–82, https://doi.org/10.3762/bjnano.5.7.

[7] O. Durante, C. Di Giorgio, V. Granata, J. Neilson, R. Fittipaldi, A. Vecchione, G. Carapella, F. Chiadini, R. DeSalvo, F. Dinelli, V. Fiumara, V. Pierro, I.M. Pinto, M. Principe, F. Bobba, Emergence and evolution of crystallization in TiO_2 thin films: a structural and morphological study, Nanomaterials 11 (6) (2021) 1409, https://doi.org/10.3390/nano11061409.

[8] D.F. Zambrano, R. Villarroel, R. Espinoza-González, N. Carvajal, A. Rosenkranz, A. G. Montaño-Figueroa, M.J. Arellano-Jiménez, M. Quevedo-Lopez, P. Valenzuela, W. Gacitúa, Mechanical and microstructural properties of broadband anti-reflective TiO_2/SiO_2 coatings for photovoltaic applications fabricated by magnetron sputtering, Sol. Energy Mater. Sol. Cells 220 (2021) 110841, https://doi.org/10.1016/j.solmat.2020.110841.

[9] X. Min Du, R.M. Almeida, Effects of thermal treatment on the structure and properties of SiO_2-TiO_2 gel films on silicon substrates, J. Sol-Gel Sci. Technol. 8 (1–3) (1997) 377–380, https://doi.org/10.1007/BF02436868.

[10] M. Waleczek, J. Dendooven, P. Dyachenko, A.Y. Petrov, M. Eich, R.H. Blick, C. Detavernier, K. Nielsch, K.P. Furlan, R. Zierold, Influence of alumina addition on the optical properties and the thermal stability of titania thin films and inverse opals produced by atomic layer deposition, Nanomaterials 11 (4) (2021), https://doi.org/10.3390/nano11041053.

[11] L. Ghazaryan, S. Handa, P. Schmitt, V. Beladiya, V. Roddatis, A. Tünnermann, A. Szeghalmi, Structural, optical, and mechanical properties of TiO_2 nanolaminates, Nanotechnology 32 (9) (2021) 095709, https://doi.org/10.1088/1361-6528/abcbc1.

[12] G.E. Testoni, W. Chiappim, R.S. Pessoa, M.A. Fraga, W. Miyakawa, K.K. Sakane, N. K.A.M. Galvão, L. Vieira, H.S. Maciel, Influence of the Al_2O_3 partial-monolayer number on the crystallization mechanism of TiO_2 in ALD TiO_2 /Al_2O_3 nanolaminates and its impact on the material properties, J. Phys. Appl. Phys. 49 (37) (2016), https://doi.org/10.1088/0022-3727/49/37/375301.

[13] R.M. Almeida, E.E. Christensen, Crystallization behavior of SiO_2-TiO_2 sol-gel thin films, J. Sol-Gel Sci. Technol. 8 (1–3) (1997) 409–413, https://doi.org/10.1007/BF02436874.

[14] G. Calleja, D.P. Serrano, R. Sanz, P. Pizarro, Mesostructured SiO_2-doped TiO_2 with enhanced thermal stability prepared by a soft-templating sol–gel route, Microporous Mesoporous Mater 111 (1–3) (2008) 429–440, https://doi.org/10.1016/j.micromeso.2007.08.021.

[15] C. He, B. Tian, J. Zhang, Thermally stable SiO_2-doped mesoporous anatase TiO_2 with large surface area and excellent photocatalytic activity, J. Colloid Interface Sci. 344 (2) (2010) 382–389, https://doi.org/10.1016/j.jcis.2010.01.002.

[16] Y. Su, J. Wu, X. Quan, S. Chen, Electrochemically assisted photocatalytic degradation of phenol using silicon-doped TiO2 nanofilm electrode, Desalination 252 (1–3) (2010) 143–148, https://doi.org/10.1016/j.desal.2009.10.011.

[17] Y.-H. Zhang, A. Reller, Phase transformation and grain growth of doped nanosized titania, Mater. Sci. Eng. C 19 (1–2) (2002) 323–326, https://doi.org/10.1016/S0928-4931(01)00409-X.

[18] Z. Zhu, S. Wu, Y. Long, L. Zhang, X. Xue, Y. Yin, B. Xu, Phase-transition kinetics of silicon-doped titanium dioxide based on high-temperature X-Ray-diffraction measurements, J. Solid State Chem. 303 (2021) 122544, https://doi.org/10.1016/j.jssc.2021.122544.

[19] H. Sankur, W. Gunning, Crystallization and diffusion in composite TiO_2-SiO_2 thin films, J. Appl. Phys. 66 (10) (1989) 4747–4751, https://doi.org/10.1063/1.343784.

[20] S. Schipporeit, M. Jerman, D. Mergel, Crystallization and conductivity of large-domain Nb-doped TiO_2 films prepared by electron beam evaporation, Thin Solid Films 754 (2022) 139299, https://doi.org/10.1016/j.tsf.2022.139299.

[21] G. Christidis, O.B. Fabrichnaya, S.M. Koepfli, E. Poloni, J. Winiger, Y. M. Fedoryshyn, A.V. Gusarov, M. Ilatovskaia, I. Saenko, G. Savinykh, V. Shklover, J. Leuthold, Photonic response and temperature evolution of SiO_2/TiO_2 multilayers, J. Mater. Sci. 56 (33) (2021) 18440–18452, https://doi.org/10.1007/s10853-021-06557-y.

[22] O. Durante, V. Granata, J. Neilson, G. Carapella, F. Chiadini, R. DeSalvo, R. De Simone, V. Fiumara, V. Pierro, I.M. Pinto, A. Vecchione, R. Fittipaldi, F. Bobba, C. Di Giorgio, Investigation of crystallization in nanolayered TiO_2-based superlattices, Surf. Interfaces 41 (2023) 103309, https://doi.org/10.1016/j.surfin.2023.103309.

[23] T. Nakayama, Structure of TiO_2/SiO_2 multilayer films, J. Electrochem. Soc. 141 (1) (1994) 237–241, https://doi.org/10.1149/1.2054690.

[24] H.-W. Pan, S.-J. Wang, L.-C. Kuo, S. Chao, M. Principe, I.M. Pinto, R. DeSalvo, Thickness-dependent crystallization on thermal anneal for titania/silica nm-layer composites deposited by ion beam sputter method, Opt. Express 22 (24) (2014) 29847, https://doi.org/10.1364/OE.22.029847.

[25] R.D.Y. Away, C. Takai-Yamashita, T. Ban, Y. Ohya, Photocatalytic properties of TiO_2-Si_22 sandwich multilayer films prepared by sol-gel dip-coating, Thin Solid Films 720 (2021) 138522, https://doi.org/10.1016/j.tsf.2021.138522.

[26] A. Hodroj, O. Chaix-Pluchery, M. Audier, U. Gottlieb, J.-L. Deschanvres, Thermal annealing of amorphous Ti–Si–O thin films, J. Mater. Res. 23 (3) (2008) 755–759, https://doi.org/10.1557/JMR.2008.0088.

[27] D.R.G. Mitchell, G. Triani, D.J. Attard, K.S. Finnie, P.J. Evans, C.J. Barbé, J. R. Bartlett, Atomic layer deposition of TiO_2 and Al_2O_3 thin films and nanolaminates, Smart Mater. Struct. 15 (1) (2006) S57–S64, https://doi.org/10.1088/0964-1726/15/1/010.

[28] L. Yang, M. Fazio, G. Vajente, A. Ananyeva, G. Billingsley, A. Markosyan, R. Bassiri, M.M. Fejer, C.S. Menoni, Structural evolution that affects the room-temperature internal friction of binary oxide nanolaminates: implications for ultrastable optical cavities, ACS Appl. Nano Mater. 3 (12) (2020) 12308–12313, https://doi.org/10.1021/acsanm.0c02798.

[29] M.C. Cisneros-Morales, C.R. Aita, Crystallization, metastable phases, and demixing in a hafnia-titania nanolaminate annealed at high temperature, J. Vac. Sci. Technol. Vac. Surf. Films 28 (5) (2010) 1161–1168, https://doi.org/10.1116/1.3474973.

[30] N.S. Gluck, H. Sankur, J. Heuer, J. DeNatale, W.J. Gunning, Microstructure and composition of composite SiO_2/TiO_2 thin films, J. Appl. Phys. 69 (5) (1991) 3037–3045, https://doi.org/10.1063/1.348591.

[31] M. Magnozzi, S. Terreni, L. Anghinolfi, S. Uttiya, M.M. Carnasciali, G. Gemme, M. Neri, M. Principe, I. Pinto, L.-C. Kuo, S. Chao, M. Canepa, Optical properties of amorphous SiO_2-TiO_2 multi-nanolayered coatings for 1064-Nm mirror technology, Opt. Mater. 75 (2018) 94–101, https://doi.org/10.1016/j.optmat.2017.09.043.

[32] J. Wang, J. Ge, H. Hou, M. Wang, G. Liu, G. Qiao, Y. Wang, Design and sol–gel preparation of SiO2/TiO2 and SiO2/SnO2/SiO2–SnO2 multilayer antireflective coatings, Appl. Surf. Sci. 422 (2017) 970–974, https://doi.org/10.1016/j.apsusc.2017.06.133.

[33] S.M. George, Atomic layer deposition: an overview, Chem. Rev. 110 (1) (2010) 111–131, https://doi.org/10.1021/cr900056b.

[34] V. Miikkulainen, M. Leskelä, M. Ritala, R.L. Puurunen, Crystallinity of inorganic films grown by atomic layer deposition: overview and general trends, J. Appl. Phys. 113 (2) (2013), https://doi.org/10.1063/1.4757907.

[35] M. Weber, A. Julbe, A. Ayral, P. Miele, M. Bechelany, Atomic layer deposition for membranes: basics, challenges, and opportunities, Chem. Mater. 30 (21) (2018) 7368–7390, https://doi.org/10.1021/acs.chemmater.8b02687.

[36] J. Peng, R. Zierold, Atomic Layer Deposition of Materials. Encyclopedia of Condensed Matter Physics, Elsevier, 2024, pp. 716–728, https://doi.org/10.1016/B978-0-323-90800-9.00206-7.

[37] S.K. Kim, G.J. Choi, J.H. Kim, C.S. Hwang, Growth behavior of Al-doped TiO2 thin films by atomic layer deposition, Chem. Mater. 20 (11) (2008) 3723–3727, https://doi.org/10.1021/cm800280t.

[38] S.K. Kim, G.J. Choi, C.S. Hwang, Controlling the composition of doped materials by ALD: a case study for Al-doped TiO2 films, Electrochem. Solid-State Lett. 11 (7) (2008) 27–30, https://doi.org/10.1149/1.2909768.

[39] L. Han, Z. Chen, High-quality thin SiO_2 films grown by atomic layer deposition using tris(Dimethylamino)Silane (TDMAS) and ozone, ECS J. Solid State Sci. Technol. 2 (11) (2013) N228–N236, https://doi.org/10.1149/2.001312jss.

[40] V.Yu Vasilyev, Review—atomic layer deposition of silicon dioxide thin films, ECS J. Solid State Sci. Technol. 10 (5) (2021) 053004, https://doi.org/10.1149/2162-8777/abffab.

[41] M. Leskelä, E. Salmi, M. Ritala, Atomic layer deposited protective layers, Mater. Sci. Forum 879 (2017) 1086–1092, https://doi.org/10.4028/www.scientific.net/MSF.879.1086.

[42] D. Bae, S. Kwon, J. Oh, W.K. Kim, H. Park, Investigation of Al2O3 diffusion barrier layer fabricated by atomic layer deposition for flexible Cu(In,Ga)Se2 solar cells, Renew. Energy 55 (2013) 62–68, https://doi.org/10.1016/j.renene.2012.12.024.

[43] T. Tokuda, Crystallization of quartz at high temperatures, Bull. Chem. Soc. Jpn. 30 (7) (1957) 692–693, https://doi.org/10.1246/bcsj.30.692.

[44] U. Holzwarth, N. Gibson, The Scherrer equation *versus* the "Debye-Scherrer Equation, Nat. Nanotechnol. 6 (9) (2011) 534, https://doi.org/10.1038/nnano.2011.145. –534.

[45] Yasaka, M. X-Ray thin-film measurement techniques. 2010.

[46] J. Schindelin, I. Arganda-Carreras, E. Frise, V. Kaynig, M. Longair, T. Pietzsch, S. Preibisch, C. Rueden, S. Saalfeld, B. Schmid, J.-Y. Tinevez, D.J. White, V. Hartenstein, K. Eliceiri, P. Tomancak, A. Cardona, Fiji: an open-source platform for biological-image analysis, Nat. Methods 9 (7) (2012) 676–682, https://doi.org/10.1038/nmeth.2019.

[47] H.-J. Gossmann, E.F. Schubert, Delta doping in silicon, Crit. Rev. Solid State Mater. Sci. 18 (1) (1993) 1–67, https://doi.org/10.1080/10408439308243415.

[48] J. Zhang, P. Zhou, J. Liu, J. Yu, New understanding of the difference of photocatalytic activity among anatase, rutile and brookite TiO_2, Phys. Chem. Chem. Phys. 16 (38) (2014) 20382–20386, https://doi.org/10.1039/c4cp02201g.

[49] O. Carp, C.L. Huisman, A. Reller, Photoinduced reactivity of titanium dioxide, Prog. Solid State Chem. 32 (1–2) (2004) 33–177, https://doi.org/10.1016/j.progsolidstchem.2004.08.001.

[50] J. Schneider, M. Matsuoka, M. Takeuchi, J. Zhang, Y. Horiuchi, M. Anpo, D. W. Bahnemann, Understanding TiO2photocatalysis: mechanisms and Materials, Chem. Rev. 114 (19) (2014) 9919–9986, https://doi.org/10.1021/cr5001892.